JCB Journal of Cell Biology

REPORT

CLAMP/Spef1 regulates planar cell polarity signaling and asymmetric microtubule accumulation in the *Xenopus* ciliated epithelia

Sun K. Kim*, Siwei Zhang*, Michael E. Werner*, Eva J. Brotslaw, Jennifer W. Mitchell, Mohamed M. Altabbaa, and Brian J. Mitchell

Most epithelial cells polarize along the axis of the tissue, a feature known as planar cell polarity (PCP). The initiation of PCP requires cell–cell signaling via the noncanonical Wnt/PCP pathway. Additionally, changes in the cytoskeleton both facilitate and reflect this polarity. We have identified CLAMP/Spef1 as a novel regulator of PCP signaling. In addition to decorating microtubules (MTs) and the ciliary rootlet, a pool of CLAMP localizes at the apical cell cortex. Depletion of CLAMP leads to the loss of PCP protein asymmetry, defects in cilia polarity, and defects in the angle of cell division. Additionally, depletion of CLAMP leads to a loss of the atypical cadherin-like molecule Celrs2, suggesting that CLAMP facilitates the stabilization of junctional interactions responsible for proper PCP protein localization. Depletion of CLAMP also affects the polarized organization of MTs. We hypothesize that CLAMP facilitates the establishment of cell polarity and promotes the asymmetric accumulation of MTs downstream of the establishment of proper PCP.

Introduction

The ability of cells to coordinately polarize across the plane of the tissue requires both cell–cell signaling through the planar cell polarity (PCP) pathway that occurs at the site of cell–cell contacts and intracellular integration of that signal via cytoplasmic changes to the cytoskeleton. The fundamental aspects of PCP signaling are conserved throughout evolution, and most of the core components were originally discovered in *Drosophila melanogaster*, where actin-based hairs and bristles project in a polarized manner in the cells of the wing and abdomen (Goodrich and Strutt, 2011). Although the global cues that set up PCP signaling remain poorly understood, there is evidence that biased microtubule-based directional trafficking can influence the establishment of PCP (Shimada et al., 2006). Furthermore, mechanical strain such as the forces generated during the tissue movements associated with gastrulation (or artificial stretching) is sufficient to facilitate PCP asymmetry (Chien et al., 2015).

Although it is generally appreciated that most epithelial cells are polarized, the lack of overtly polarized structures limits the number of cell types that have been useful for experimental analysis. In vertebrates, the coordination of cell polarity is exquisitely displayed in multiciliated cells (MCCs) found in ciliated epithelia such as the trachea, the oviduct, and the ependyma, all of which produce a polarized cilia driven fluid flow. The proper polarization of cilia is well known to require PCP signaling (Park et al., 2008; Mitchell et al., 2009; Guirao et al., 2010; Vladar et al., 2012; Boutin et al., 2014). Additionally, shear stress, mechanical stress, and microtubule (MT) and actin dynamics all coordinate to produce MCCs with properly aligned cilia (Mitchell et al., 2007; Guirao et al., 2010; Werner et al., 2011; Vladar et al., 2012; Chien et al., 2015). In humans, the genetic loss of polarized cilia-driven fluid flow results in an increased risk for hydrocephaly, infertility, and respiratory infections (Bush and Hogg, 2012). Moreover, PCP signaling drives numerous developmental events including gastrulation, convergent extension, and neural tube formation (Wallingford, 2005a,b). Here we identify a novel regulator of PCP signaling, CLAMP/Spef1, that modulates cell–cell communication via the atypical cadherin, Celsr2, and facilitates asymmetric PCP protein localization and downstream asymmetric MT function.

CLAMP is a MT-associated protein that dynamically associates with the MT lattice and stabilizes MTs (Chan et al., 2005; Dougherty et al., 2005; Werner et al., 2014). In *Xenopus laevis*, CLAMP has been previously implicated in the apical accumulation of stable acetylated MTs that are required during the process of radial intercalation by which MCCs and ionocytes undergo polarized migration from an inner epithelial layer into the outer epithelium (Werner et al., 2014). However, in addition to the

Department of Cell and Molecular Biology, Feinberg School of Medicine, Northwestern University, Chicago, IL.

*S.K. Kim, S. Zhang, and M.E. Werner contributed equally to this paper; Correspondence to Brian J. Mitchell: brian-mitchell@northwester.edu; Siwei Zhang's present address is Center for Psychiatric Genetics, NorthShore University HealthSystem, Evanston, IL; Michael E. Werner's present address is Dept. of Biology, University of North Carolina at Chapel Hill, Chapel Hill, NC.

https://doi.org/10.1083/jcb.201706058

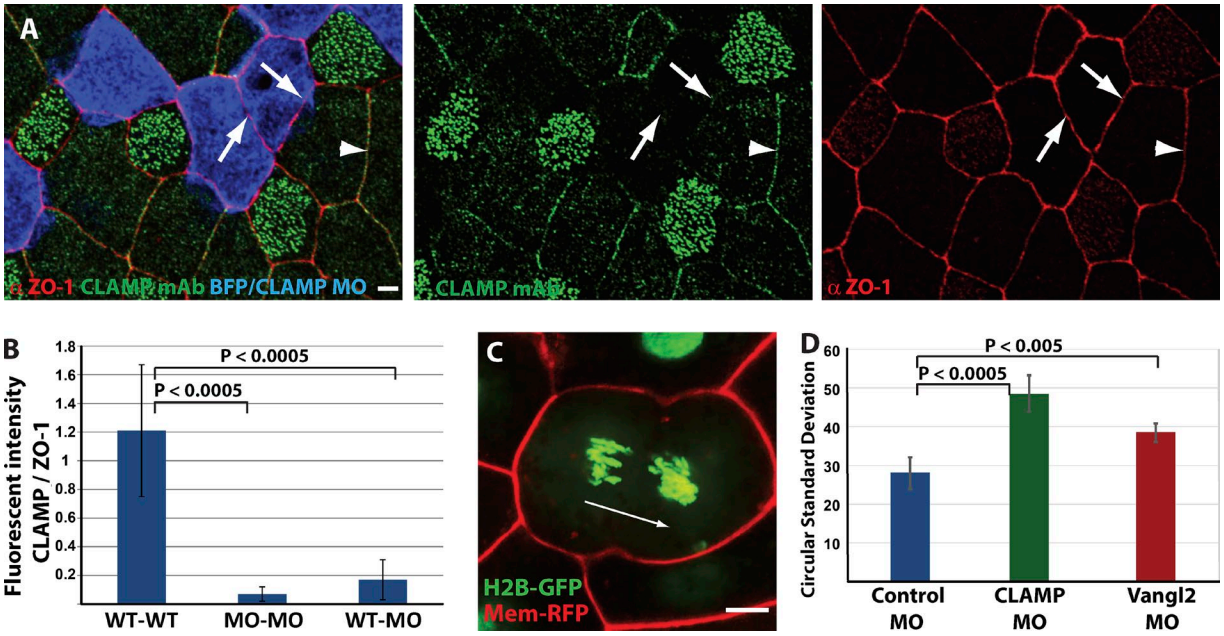

Figure 1. **CLAMP depletion has a non–cell-autonomous effect on CLAMP membrane localization and polarized cell division. (A)** Ab staining of CLAMP mAb (green) and ZO-1 (red) reveal a strong association of CLAMP to the cell cortex. In mosaic tissues where CLAMP MO is marked with blue fluorescent protein (BFP, blue), CLAMP mAb staining is lost within and at the borders of CLAMP morphants and WT cells (blue; arrows) relative to WT–WT boundaries (arrowhead). **(B)** Quantification of fluorescent intensity of CLAMP mAb relative to ZO-1 Ab at the WT–WT boundary (n = 43), MO–MO (n = 42) and WT–MO (n = 82) cells in CLAMP morphant mosaic tissues. **(C and D)** Quantitative analysis (D) of the angle of cell division (representative image, C) measuring the CSD relative to the A-P axis in control MO (n > 500 cells from seven embryos), CLAMP MO (n > 300 cells from seven embryos) and Vangl2 MO cells (n > 700 cells from six embryos). In both B and D, error bars represent the SD, and p-values represent the t test (two-tailed, type 2). In all images, posterior is to the right. Bars, 5 µm.

association with MTs, we find that there is a significant enrichment of CLAMP at non-MT sites, including the rootlets associated with motile cilia and the sites of apical cell–cell junctions (Fig. 1 A). We hypothesize that this junctional pool of CLAMP is used in multiple forms of cell polarity by modulating PCP protein stability and localization. Additionally, MT function is influenced by PCP signaling, and we find multiple defects in MTs downstream of both CLAMP and PCP signaling, indicating an additional, indirect role for CLAMP in facilitating MT dynamics.

Results and discussion

Immunostaining with a CLAMP-specific mAb indicates that CLAMP weakly localizes to the MT network and enriches at sites of increased MT concentration (e.g., midbodies, centrioles, and cilia; Werner et al., 2014). Importantly, CLAMP also enriches at the apical cell membrane at the site of cell–cell contacts (Fig. 1 A). To test whether this enrichment at cell boundaries is specific, we generated mosaic embryos in which cells marked with blue fluorescent protein contained a previously validated CLAMP morpholino (MO; Werner et al., 2014). Immunofluorescence confirms that CLAMP staining in CLAMP morphant cells is largely absent (Fig. 1, A and B). We quantified this loss specifically at cell contacts by scoring the fluorescent intensity of CLAMP relative to the tight junction marker ZO-1 at apical junctions and found a >90% decrease in CLAMP staining at MO–MO boundaries compared with WT–WT boundaries (Fig. 1 B; P < 0.0005). More importantly, when we performed this analysis between WT–MO boundaries, we also saw a significant loss of CLAMP staining, indicating a non–cell-autonomous effect where loss of membrane-associated CLAMP in one cell leads to a loss of membrane-associated CLAMP in its neighbor (Fig. 1 B; P < 0.0005).

CLAMP has been previously implicated in the radial intercalation of MCCs and ionocytes, yet antibody (Ab) staining reveals that it is expressed throughout all cells of the epithelium. A high dose of CLAMP MO (10 ng in each blastomere at the 4-cell stage) causes early embryonic lethality around stage 14 before MCC differentiation. Consistent with this, our attempts at CRISPR-mediated genome editing also resulted in a complete loss of viability, suggesting a broad developmental role for CLAMP. Importantly, targeted injections of MOs into a subset of blastomeres (1 cell at the 4-cell stage) generates mosaic embryos that exhibit a much higher survival rate and allow for the comparison of WT and morphant cells in the same embryo (Werner and Mitchell, 2013). In fact, mosaic CLAMP morphant embryos often exhibit an overall stunted and curved growth reminiscent of PCP-mediated convergent extension defects (Wallingford et al., 2002). We observe that during embryo elongation (stages 16–28), the majority of mitotic cells align their spindles along the anterior–posterior (A-P) axis with a circular SD (CSD) of 27° (Fig. 1, C and D). Similar to what has been observed in other elongating tissues, we observe that spindle orientation is sensitive to PCP signaling (Vichas and Zallen, 2011). Disruption of PCP using a previously validated Vangl2 MO leads to a significant increase in CSD relative to control (Fig. 1 D; CSD, 38°; P < 0.005; Mitchell et al., 2009). Consistent with CLAMP having a role in PCP signaling, we also observe that CLAMP depletion leads to a similar defect in spindle orientation (Fig. 1 D; CSD, 48°; P < 0.00005).

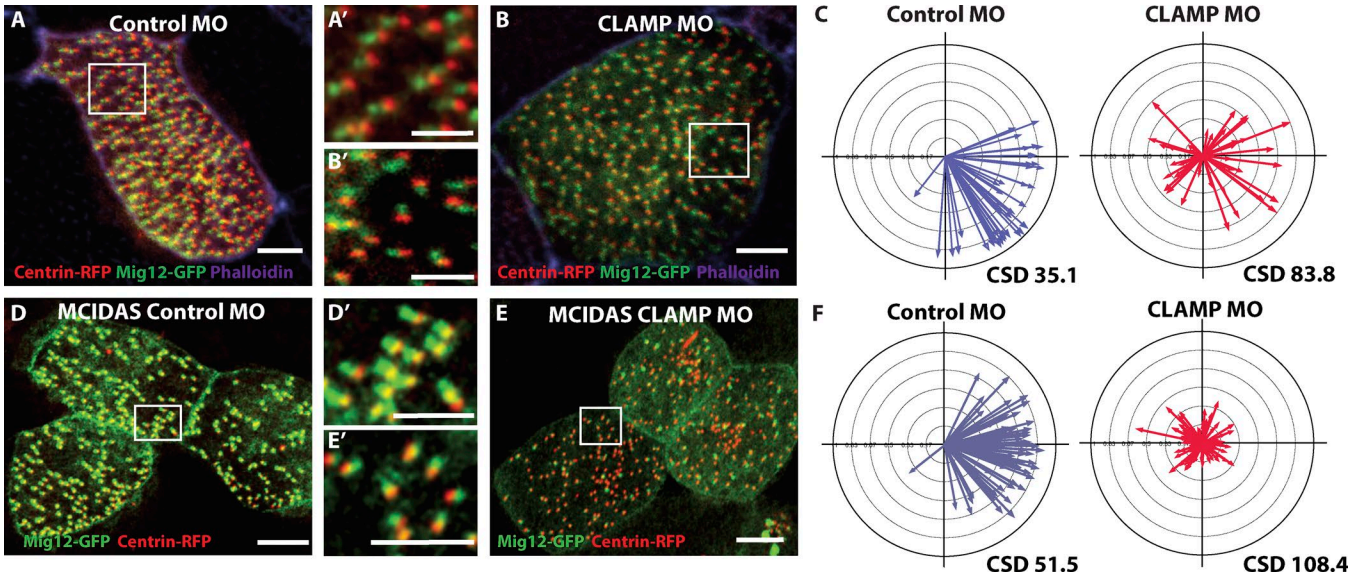

Figure 2. **CLAMP affects cilia and MCC polarity. (A and B)** Cilia polarity as assessed by the position of the rootlet marked with Mig12-GFP (green) relative to basal body marked with centrin4-RFP (red) in control MO (A) and CLAMP MO 5 ng (B) cells. Insets (A′ and B′) show the orientation of individual cilia. In all pictures and in all the quantification throughout the paper, anterior is to the left and posterior is to the right. **(C)** Quantification of morphant MCC polarity (n = 46 cells for each condition) as scored by the mean cilia direction within each cell (arrow direction) and the variation around that mean (arrow length such that long arrow represents low variance). **(D–F)** Similar analysis to A–C done on ectopic MCCs induced by the expression of MCIDAS using mosaic tissue injected with 10 ng of MO (n = 61 cells for control MO and 82 for CLAMP MO). Posterior is to the right. Bars: 5 µm; (insets) 2.5 µm.

In MCCs that are properly polarized, cilia beat in the posterior direction, which is reflected in their striated rootlets projecting in the anterior direction (Park et al., 2008). Partial depletion of CLAMP using 5 ng of MO in one of the four blastomeres results in a phenotype where a substantial number of MCCs manage to intercalate properly, thus allowing us to score cilia polarity. We determined polarity in these cells by scoring the position of the rootlets (marked with Mig12-GFP) and their associated basal bodies (marked with Centrin-RFP) relative to the A-P axis (Fig. 2; Park et al., 2008). We observe two distinct polarity defects. First, there is a significant loss of coordination of cilia polarity within cells (Fig. 2, A and B; and Fig. 1 C, length of arrow; mean vector length of 0.82 in control vs. 0.38 in CLAMP morphants). Quantification of this phenotype shows an increase in the CSD of 83.8° for CLAMP morphants compared with 35.1° for control morphants ($P < 0.0005$). This is similar to what has been reported for cells treated with the MT depolymerizing drug nocodazole, consistent with the idea that CLAMP is required for regulating MT stability during the establishment of cilia polarity (Werner et al., 2011). In addition, we also observe a randomization in the mean cilia orientation, which has been used as a proxy for cell polarity (Fig. 2 C, direction of arrows; Werner and Mitchell, 2012). In fact, the loss of mean cilia orientation has previously been associated with defects of PCP signaling consistent with CLAMP affecting the PCP pathway (Park et al., 2008; Mitchell et al., 2009; Guirao et al., 2010; Vladar et al., 2012; Boutin et al., 2014).

To address the possibility that the observed polarity defects are the result of subtle defects in MCC intercalation, we circumvented the intercalation defects by converting outer epithelial cells (OCs) into MCCs using the MCC differentiation factor Multicilin (or MCIDAS; Stubbs et al., 2012). In ectopic MCCs injected with control MO, polarity is well established (Fig. 2, D and F; mean vector, 0.66; CSD, 51.5°). In contrast, when ectopic MCCs were depleted of CLAMP (10 ng into one blastomere), we found a severe loss in both directionality and coordination (Fig. 2, E and F; mean vector, 0.19; CSD, 108.4°; $P < 0.0005$). Collectively, these results suggest that CLAMP is required for proper PCP-dependent establishment of cilia polarity.

When properly polarized, epithelial cells display asymmetric accumulation of core PCP proteins (Goodrich and Strutt, 2011). A complex of the transmembrane protein Frizzled (Fz) with Disheveled (Dvl) localizes to one side of the cell, whereas a complex of the transmembrane protein Strabismus/Van Gogh (Vangl) together with Prickle (Pk) localizes to the other. These asymmetric complexes are both stabilized and strengthened by interactions with members of the Flamingo/Celsr family of transmembrane atypical cadherins (Strutt et al., 2016). In *Xenopus*, PCP asymmetry is exemplified by the accumulation of GFP-tagged Pk2 at the apical cell cortex on posterior cell boundaries and GFP-tagged Dvl1 at anterior boundaries (Fig. 3, A, C, F–H, and J; and Fig. S1 A; Butler and Wallingford, 2015). To test the hypothesis that CLAMP functions in establishing PCP, we measured the fluorescent intensity at the anterior versus posterior cell boundary of GFP-Pk2– and Dvl1-GFP–expressing cells and found that asymmetric accumulation of these proteins is lost in CLAMP morphant cells (Fig. 3, B, F, I, and J; and Fig. S1, A–C). Interestingly, we do not see a loss or change in CLAMP staining in Vangl2-deficient cells (Fig. S1, E and F). Therefore, although CLAMP regulates PCP signaling via localization of asymmetric PCP components, the reciprocal does not appear to be true, suggesting that CLAMP is upstream of PCP signaling.

A hallmark of PCP signaling is the non–cell-autonomous defects that propagate when PCP molecules are disrupted. We tested for a non–cell-autonomous effect using mosaic tissues

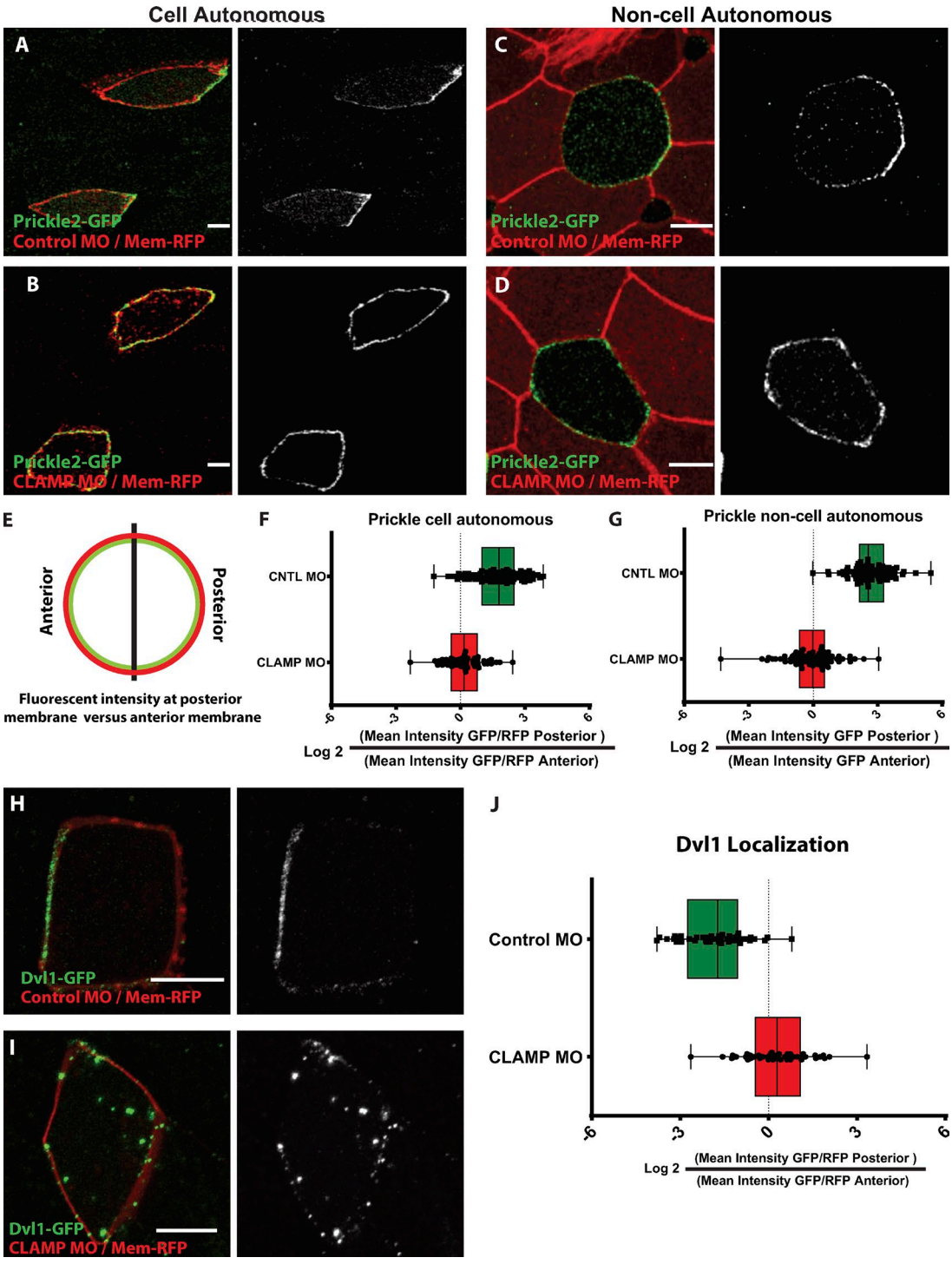

Figure 3. **CLAMP controls PCP protein asymmetry. (A–G)** GFP-Pk2 (green) asymmetrically accumulates on the posterior side of cells (A and C) which we quantify (n > 50 cells for each condition) by measuring the fluorescent intensity on the posterior side versus the anterior side (E–G) of control (CNTL) cells (relative to mem-RFP, red, in F). This asymmetry is lost in CLAMP morphant tissues marked with mem-RFP (red) both cell-autonomously (A, B, and F) and non–cell-autonomously (C, D, and G). **(H–J)** Dvl1-GFP (green) asymmetrically accumulates on the anterior side of cells (H and J), which we quantify by measuring the fluorescent intensity on the posterior side versus the anterior side (J) of the cell relative to mem-RFP (red) in control MO (n = 82 cells) and CLAMP MO (n = 36 cells). Graphs are whisker plots where the error bars represent the range; the line in the box represents the median and the box represents the upper and lower quartile. Posterior is to the right. Bars, 5 µm.

expressing GFP-Pk2 in which a subset of cells were depleted of CLAMP (marked by mem-RFP). In isolated morphant cells (cell-autonomous Fig. 3, B and F) as well as WT cells surrounded by morphants tissue (non–cell-autonomous; Fig. 3, D and G), there is a failure to localize Pk2 asymmetrically. This non–cell-autonomous effect is bidirectional, as we observe Pk2 defects in cells bordering CLAMP morphants on either the posterior or anterior side (Fig. S1 D). Importantly, we also find CLAMP-mediated

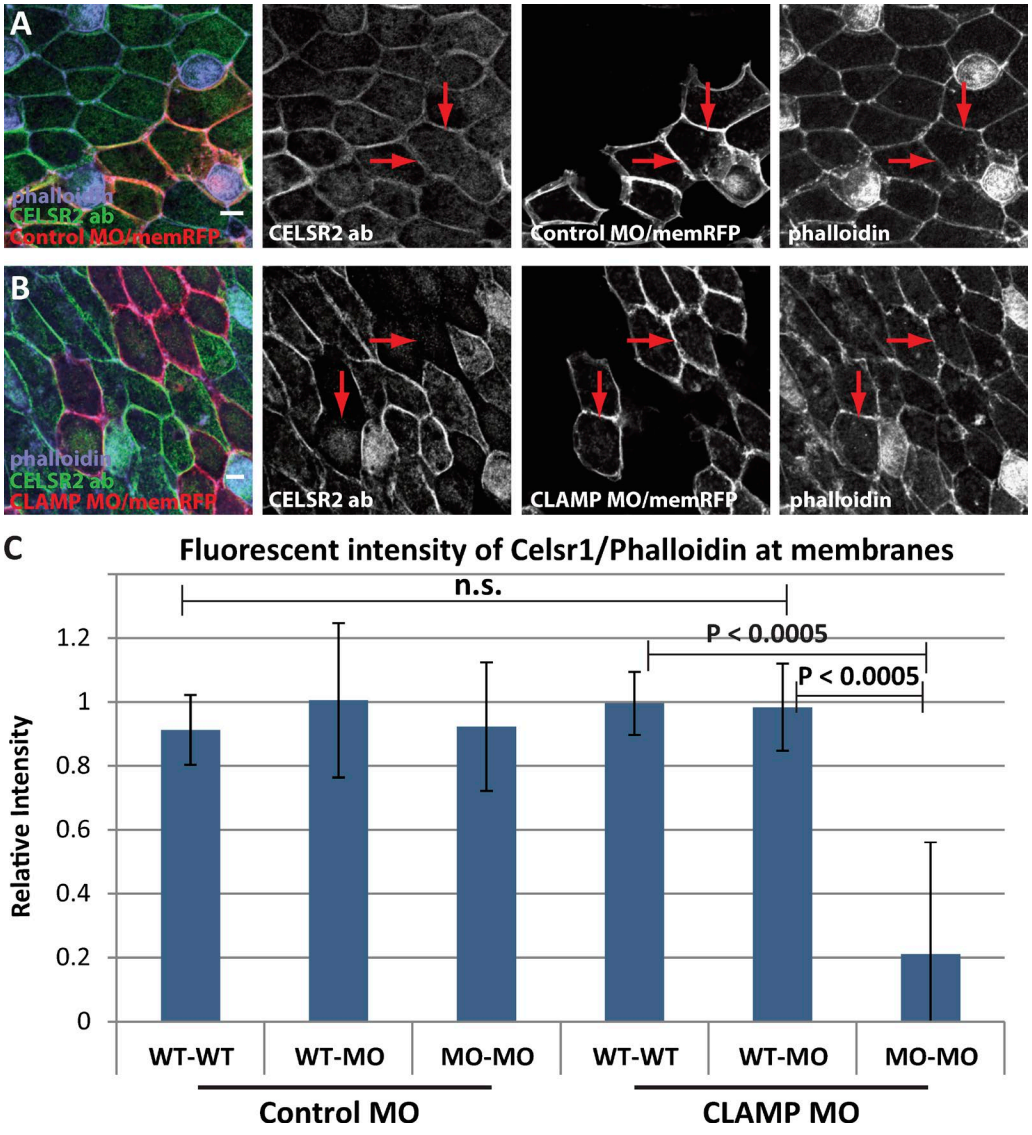

Figure 4. **CLAMP depletion affects Ceslr2 membrane localization. (A and B)** Ceslr2 Ab staining (green/white) in mosaic tissues injected with mem-RFP together with control MO (A) or CLAMP MO (B) (red/white) with cell membranes marked with phalloidin (purple/white). **(C)** Quantification of Ceslr2 fluorescent intensity relative to phalloidin at cell contacts between WT–WT (n = 8), WT–MO (n = 7), and MO–MO (n = 10) cells. Error bars represent the SD, and p-values represent the t test (two-tailed, type 2). Bars, 10 µm.

PCP defects in both MCCs and OCs, suggesting that CLAMP is broadly used to establish and transmit PCP signaling cues (Fig. S1, A–C). CLAMP localizes symmetrically around the cell cortex, and CLAMP depletion causes a bidirectional loss of CLAMP and proper PCP signaling in neighboring cells. These results suggest that CLAMP could modulate cell–cell interactions that facilitate PCP signaling. Celsrs form complexes with both Fz-Dvl on one side of the cell and with Vangl-Pk on the other and act to coordinately stabilize bidirectional PCP signaling (Tissir and Goffinet, 2013; Strutt et al., 2016). Using a previously published *Xenopus* Celsr2 Ab (Cha et al., 2011), we tested the effect of CLAMP depletion on Celsr2 localization. Depletion of CLAMP leads to a significant loss of Celsr2 in morphant cells (Fig. 4; WT-WT vs. MO–MO; P < 0.0005). Importantly, the depletion of CLAMP does not have a non–cell-autonomous effect on Celsr2 in neighboring cells, suggesting that the non–cell-autonomous loss of CLAMP is not strictly mediated via Celsr2 (Fig. 4, B and C). To further explore this, we generated a Celsr2 MO and found that Celsr2 depletion led to an expected depletion of Ceslr2 at membranes between MO–MO cells (vs. WT-WT; P < 0.0005) and a partial depletion between WT–MO cells (Fig. S2, A–C; vs. WT-WT; P < 0.05). In contrast, depletion of Ceslr2 had no effect on CLAMP localization, further suggesting that CLAMP function is upstream of Celsr2 and PCP signaling (Fig. S2, D–F). In mouse ependymal cells, Celsr1-3 have distinct polarity roles that combine to facilitate the proper polarization of MCCs with Celsr1, driving tissue level coordination, and Celsr2 and 3, driving cilia coordination (Boutin et al., 2014). Although our analysis focused on Celsr2, CLAMP depletion affects multiple aspects of polarity, suggesting it may similarly affect other Celsr family members.

CLAMP binds and stabilizes MTs, suggesting that the mechanism for modulating PCP signaling could be mediated via MTs.

Alternatively, CLAMP could regulate PCP asymmetry, which in turn could regulate MT function. In fact, MTs are known to act both upstream of PCP signaling by facilitating the asymmetric accumulation of PCP components and downstream of PCP signaling by accumulating asymmetrically in a PCP-dependent manner (Shimada et al., 2006; Vladar et al., 2012). In mouse tracheal and ependymal MCCs, treatment with nocodazole leads to a loss of PCP protein asymmetry (Vladar et al., 2012; Boutin et al., 2014). Importantly, treating *Xenopus* embryos between stages 20 and 28, using a dose of nocodazole that stunts proper cilia formation, did not lead to quantifiable changes in Celsr2 membrane accumulation (Fig. S3, A–C). We interpret this result as indicating a function of CLAMP at the membrane that is distinct from its role in stabilizing MTs. However, the critical window of PCP formation is unknown, and the continued development of embryos in our experiments indicates that MT dynamics were not completely abolished, leaving open the possibility that MTs could potentially play a role in CLAMP-mediated Celsr2 localization.

In *Xenopus*, MTs form a dense apical network connecting the dozens of basal bodies in MCCs (Werner et al., 2011). Using the MT binding domain of Ensconsin fused to GFP (EMTB-3xGFP) as a proxy for MTs, we observe that this apical MT network comes into close proximity of the cell membrane at the posterior cell border and that there is a small but reproducible gap at the anterior cell boundary (Fig. 5 A). We quantified this phenotype by measuring the fluorescent intensity of EMTB-3xGFP within 1 µm of the cell membrane on the posterior versus anterior side of the cell at the level of basal bodies (Fig. 5, D and E). The posterior enrichment seen in control morphants is lost in CLAMP morphant cells, and in the majority of these cells, the MT network organizes uniformly around the cell membrane (Fig. 5, B and E). Given the feedback between the PCP pathway and MTs, this phenotype could be either upstream or downstream of PCP signaling. To test this, we quantified EMTB-3xGFP in Vangl2 morphants and found a similar loss of MT asymmetry, suggesting that this phenotype is downstream of both CLAMP and PCP function (Fig. 5, C and E). Consistent with this, we only see this asymmetry in mature MCCs that have completed polarization (e.g., stage 28).

MTs are inherently polarized with a predominantly stable (–) end and a dynamic (+) end. We generated a GFP fusion to the MT (–) end protein CAMSAP2 (CAMSAP2-GFP) and found that in OCs, CAMSAP2 localized to punctate foci throughout the cell (Fig. S3 D, arrows; Hendershott and Vale, 2014; Jiang et al., 2014). In contrast, there is a strong preferential accumulation of CAMSAP2 in filaments throughout the posterior side of MCCs (Fig. 5, F and F′; and Fig. S3 D). To quantify this phenotype, we created confocal stacks of CAMSAP2-GFP, measured the fluorescent intensity on each side of the cell, and found a substantial posterior enrichment of CAMSAP2 in control cells that was completely abolished in CLAMP morphant cells (Fig. 5, F–I). The contrast of phenotypes is evident in mosaic tissues in which a WT cell can be seen in close proximity to a CLAMP morphant marked by blue dextran (Fig. 5 G). Importantly, we do not observe any enrichment of CLAMP at the CAMSAP2-labeled MTs. Furthermore, this pool of MTs is distinct from the network of MTs linking basal bodies to the cell cortex as it is enriched throughout the entire posterior side of the cell and not just the apical cortex (Fig. 5 F′, side projection). Additionally, similar to the EMTB data, we only observe CAMSAP2 asymmetry in MCCs that have already established cell polarity (e.g., stage 28), suggesting it is downstream of PCP signaling. To address this hypothesis, we tested CAMSAP2 localization in Vangl2 morphants and found a loss of asymmetry similar to depletion of CLAMP (Fig. 5 I and Fig. S3 E). Unlike (+) end markers, which are restricted to the growing tip, CAMSAP2 decorates part of the microtubule lattice at the (–) portion of the MT, not just the (–) tip (Hendershott and Vale, 2014; Jiang et al., 2014). As such, the CAMSAP2 localization reveals a distinct stable subset of the MT network that appears to run along the posterior cell membrane dependent on CLAMP-mediated PCP. Collectively, these data suggest that CLAMP promotes the asymmetric distribution of both membrane-associated PCP proteins and a stable subset of the MT network that is asymmetrically positioned within the cytoplasm.

CLAMP has been previously implicated in the asymmetric accumulation of stable MTs during radial intercalation, where it promotes the directional movements of MCCs and ionocytes into the outer epithelium. Here we identify a novel role for CLAMP in promoting PCP, suggesting that CLAMP is broadly used to facilitate multiple forms of cell polarity. Overall, our results implicate CLAMP as a novel regulator of PCP signaling. We propose that CLAMP facilitates cell–cell communication, as indicated by its role in Celsr2 localization, which in turn promotes the formation of asymmetric PCP protein complexes. The asymmetric accumulation of differential PCP complexes on opposite sides of the cell is a complex process that has been proposed to require differential trafficking, differential junctional stabilization, differential endocytic recycling, and competitive protein interactions that asymmetrically influence these processes (Butler and Wallingford, 2017). In fact, although Celsr forms homophilic interactions with other Celsr molecules, it preferentially stabilizes those interactions if they are between Celsr-Fz-Dvl and Celsr-Vangl-Pk complexes (Strutt and Strutt, 2008). Interestingly, in CLAMP morphant, cells we see Pk2 accumulate symmetrically around the cell cortex (Fig. 3 B). In contrast, although Dvl1 is also distributed symmetrically, we see a substantial loss of Dvl1 at the membrane, suggesting that Dvl1 either is not properly trafficking to the cortex or is being inappropriately endocytosed (Fig. 3 I).

It is certainly curious that in mosaic CLAMP morphants, junctional CLAMP is lost from WT neighboring cells whereas Celsr2 remains. The partial depletion of Celsr2 at Celsr2 MO–WT boundaries (Fig. S2 C) compared with normal Ceslr2 levels at CLAMP MO–WT boundaries (Fig. 4) suggests that CLAMP's effect is not strictly via modulating Celsr2 protein levels but more likely reflects a function in modulating differential Celsr complexes. Future work will be required to determine if CLAMP functions to differentially modulate trafficking or endocytosis or whether it specifically stabilizes particular PCP junctional complexes.

Materials and methods

Embryo injections, plasmids, mRNA, and MOs

The synthesis and injection of plasmid DNA, mRNA, and MOs into early *Xenopus* embryos were performed using standard

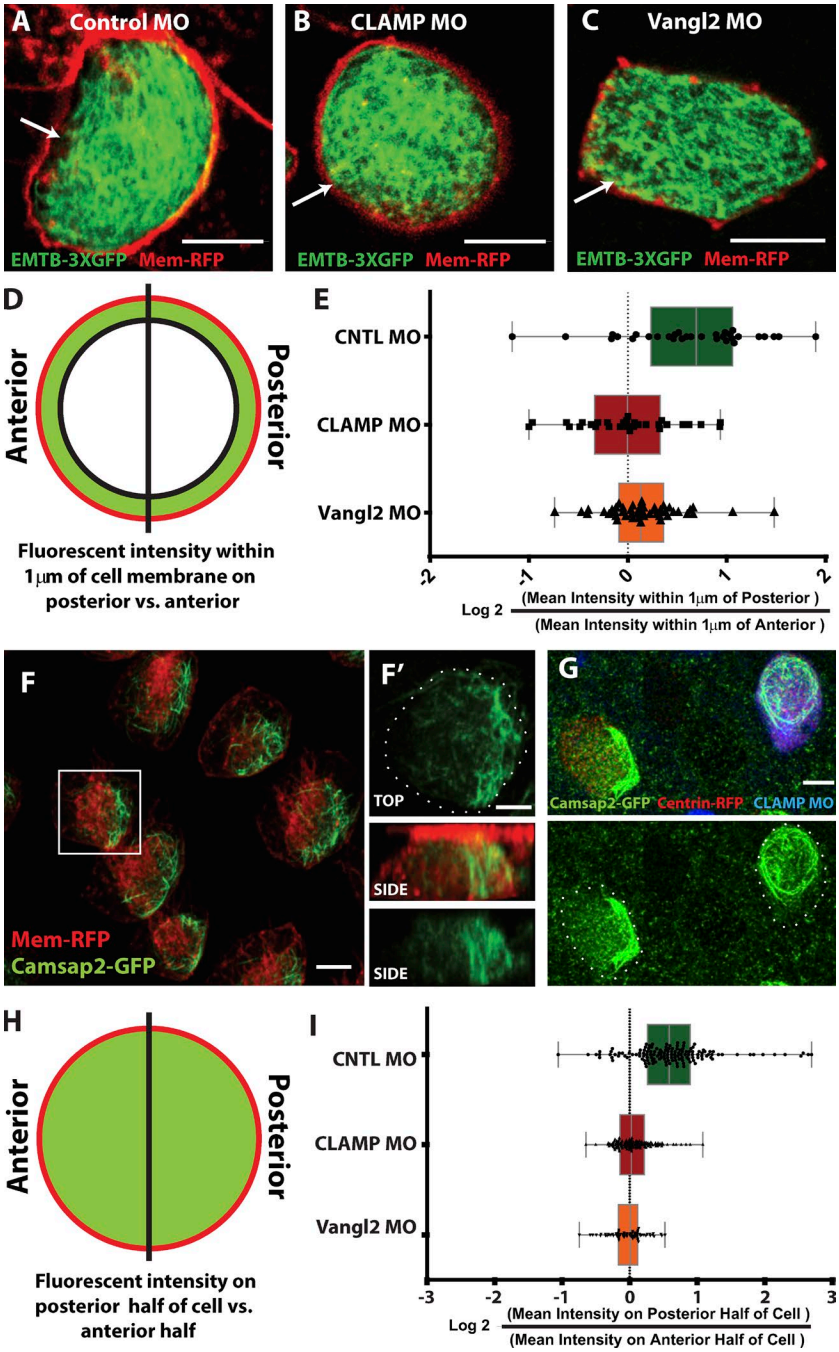

Figure 5. **CLAMP depletion affects microtubule asymmetry. (A–C)** Imaging of microtubules using the EMTB-3xGFP (green) relative to the cell cortex marked with mem-RFP (red) reveals a gap between the microtubules and the cortex at the anterior side of the cell but not the posterior side that is lost in both CLAMP (B) and Vangl2 (C) morphant cells. **(D and E)** This phenotype was quantified by measuring the mean fluorescent intensity of EMTB-3xGFP within 1 µm of the cell cortex on the posterior side relative to the anterior side (D) in control (n = 33 cells), CLAMP (n = 30 cells), and Vangl2 (n = 48 cells) morphant cells at the level of the basal bodies (E). **(F–I)** Confocal stacks (~8 µm deep) of CAMSAP2-GFP (green, F and F′ top and F′ side) reveal a posterior (to the right) bias in MCCs (red; RFP driven by the α-tubulin promoter) that projects across the entire posterior side of the cell (F′ top and side). Mosaic tissue showing a loss of CAMSAP2 (green) asymmetry in CLAMP morphant MCC marked with dextran (blue) compared with a WT MCC (green only; G). Quantification of the CAMSAP2 phenotype measuring the mean fluorescent intensity of CAMSAP2 within the posterior half of the cell relative to the anterior half (H) in control (n = 143 cells), CLAMP (n = 136 cells), and Vangl2 (n = 77 cells) morphant cells (I). Graphs are whisker plots where the error bars represent the range; the line in the box represents the median and the box represents the upper and lower quartile. In all images, posterior is to the right. Bars: 5 µm; (inset) 2.5 µm.

protocols approved by the Northwestern University Institutional Animal Care and Use Committee (Werner and Mitchell, 2013; Zhang and Mitchell, 2015). Plasmids were linearized with NotI, and mRNA was generated by in vitro transcription using SP6 RNA polymerase as previously described (Sive et al., 1998). For scoring cilia polarity, Centrin4-RFP and GFP/RFP-CLAMP mRNAs were injected to mark the basal bodies and rootlets, respectively (Klos Dehring et al., 2013; Werner et al., 2014). To score PCP polarity, we injected mRNA generated from pCSDEST-GFP-PK2, pCSDEST-Dvl1-GFP, and pCSDEST-Dvl2-GFP, which were gifts from the Wallingford Lab (Butler and Wallingford, 2015). MCIDAS experiments were performed using injection of a dexamethasone-inducible version of MCIDAS (hGR-MCI) followed by treatment of dexamethasone between stages 12 and 20 to induce the formation of MCCs (Stubbs et al., 2012). pTub-GFP-Pk2 and pTub-Dvl1-GFP were cloned from the above-mentioned plasmids and subsequently cloned into pCS2Tub vector linearized by ClaI using Gibson Assembly and injected as DNA. Similar protocols were also applied in constructing the pTub–membrane RFP (mem-RFP). pCS107-hCAMSAP2-GFP was cloned from pMT-CAMSAP2-GFP from the Akhmanova laboratory using Gibson Assembly (Jiang et al., 2014). MOs (Gene Tools, LLC) used were control MO (5′-CCT CTTACCTCAGTTACAATTTATA-3′), CLAMP MO (5′-TCTCCTCAT CAAACTCCACCGCCAT-3′), and Vangl2 MO (5′-ACTGGGAATCGT TGTCCATGTTTC-3′; Mitchell et al., 2009; Werner et al., 2014). For drug treatment, the concentration of nocodazole (0.3 µM)

was the highest dose that affected MTs as scored by cilia formation and CLIP-170 dynamics but did not completely block development. Embryos were treated with 0.3 µM nocodazole, or the equivalent amount of DMSO for control, overnight from stage 18 to stage 28 at 18°C followed by fixation.

Immunofluorescence, microscopy, and quantification

Embryos were fixed in either 4% PFA in PBS for 2 h or 100% methanol for 48 h at −20°C (required for anti-CLAMP; Werner and Mitchell, 2013; Zhang and Mitchell, 2015). Abs used were anti–ZO-1 (61–7300; Thermo), anti-CLAMP (Werner et al., 2014), anti-CELSR2 (Cha et al., 2011), and Cy-2–, Cy-3–, or Cy-5–conjugated secondary Abs (Jackson ImmunoResearch Laboratories, Inc.). The Celsr2 Ab we used was a gift from S.W. Cha (Cincinnati Children's Hospital, Cincinnati, OH) that was previously published (Cha et al., 2011). However, in that publication, Celsr2 was incorrectly referred to as Celsr1. The sequences used to verify Ab specificity were GCAGCAACTCAGGATGTTCA and TTTATTCCACGCAGGGTC TC, both of which correspond to Celsr2 (Cha et al., 2011). Additionally, we generated both Celsr1 and Celsr2 MOs but only saw a loss of Ab staining in the Celsr2 MO embryos. To visualize actin, we used phalloidin 568 or 647 (Invitrogen) GFP-PK2 and Dvl1-GFP data were captured on live embryos (Butler and Wallingford, 2015). Confocal images were taken using Nikon Elements software on a Nikon A1R microscope with 60× Plan/Apo, 1.4 NA oil objective lens. Live and fixed imaging was performed at room temperature in 0.1× Marc's Modified Ringer's for live or in Fluoro-gel for fixed (Electron Microscopy Sciences). The quantification of rootlet orientation, cell shape, and cell polarity was manually conducted using Nikon Elements software. Oriana2 was used for all circular statistics and graphing. Quantification of fluorescent intensity was performed as described in legends using Nikon Elements software (Fig. 1 B; Fig. 2, F, G, and J; Fig. 4 C; Fig. S1, C, D, and F; Fig. S2 D; and Fig. S3 C) or using ImageJ (Fig. 5, E and I; and Fig. S2 C). In brief, intensity measurements were taken at the cell membrane marked by phalloidin, mem-RFP, or ZO-1 (Fig. 1 B; Fig. 3, F, G, and J; Fig. 4 C; Fig. S1, C and D; and Fig S3 C) within 1 µm of the cell membrane (Fig. 5 E), or within the entire half of the cell (Fig. 5 I). Localization graphs (Fig. 3, F, G, and J; Fig 5, E and I; and Fig. S1, C and D) were plotted using GraphPad from the log2 value of posterior intensity/anterior intensity as described in the figures (Fig. 3, Fig. 5, and Fig. S1; Butler and Wallingford, 2015). Excel (Microsoft) was used for noncircular statistics and bar graphs. In bar graphs (Fig. 1, B and D; Fig. 4 C; Fig. S1 F; Fig S2, C and D; and Fig. S3 C), the error bars represent the SD and the p-values were calculated using two-tailed type 2 *t* tests. Data distribution was assumed to be normal, but this was not formally tested.

Online supplemental material

Fig. S1 shows that CLAMP depletion disrupts Pk-2 asymmetric localization in OCs and non–cell-autonomously in WT neighboring cells. Additionally, CLAMP localization appears normal in PCP-defective cells. Fig. S2 shows that Celsr2 depletion leads to a loss of Celsr2 from membranes but not a loss of CLAMP. Fig. S3 shows that treatment of embryos with nocodazole does not change Celsr2 membrane association and that CAMSAP2 asymmetric accumulation is lost in PCP-defective cells.

Acknowledgments

Thanks to John Wallingford for constructs, and Chad Pearson and Eszter Vladar for critical reading of the manuscript.

M.E. Werner was supported by a fellowship from the American Heart Association. B.J. Mitchell was a Whitman Fellow at the Marine Biological Laboratories at Woods Hole and received the Nikon Imaging Fellowship (2016). This research was supported by a National Institutes of Health–National Institute of General Medical Sciences grant to B.J. Mitchell (R01GM089970).

The authors declare no competing financial interests.

Author contributions: S.K. Kim, S. Zhang, and M.E. Werner all contributed intellectually to the development of this project and performed the majority of critical experiments. E.J. Brotslaw, J.W. Mitchell, and M.M. Altabbaa all performed experiments and quantifications for numerous experiments. B.J. Mitchell conceived and supervised the project.

Submitted: 9 June 2017
Revised: 1 January 2018
Accepted: 12 February 2018

References

Boutin, C., P. Labedan, J. Dimidschstein, F. Richard, H. Cremer, P. André, Y. Yang, M. Montcouquiol, A.M. Goffinet, and F. Tissir. 2014. A dual role for planar cell polarity genes in ciliated cells. *Proc. Natl. Acad. Sci. USA.* 111:E3129–E3138. https://doi.org/10.1073/pnas.1404988111

Bush, A., and C. Hogg. 2012. Primary ciliary dyskinesia: recent advances in epidemiology, diagnosis, management and relationship with the expanding spectrum of ciliopathy. *Expert Rev. Respir. Med.* 6:663–682. https://doi.org/10.1586/ers.12.60

Butler, M.T., and J.B. Wallingford. 2015. Control of vertebrate core planar cell polarity protein localization and dynamics by Prickle 2. *Development.* 142:3429–3439. https://doi.org/10.1242/dev.121384

Butler, M.T., and J.B. Wallingford. 2017. Planar cell polarity in development and disease. *Nat. Rev. Mol. Cell Biol.* 18:375–388. https://doi.org/10.1038/nrm.2017.11

Cha, S.W., E. Tadjuidje, C. Wylie, and J. Heasman. 2011. The roles of maternal Vangl2 and aPKC in Xenopus oocyte and embryo patterning. *Development.* 138:3989–4000. https://doi.org/10.1242/dev.068866

Chan, S.W., K.J. Fowler, K.H. Choo, and P. Kalitsis. 2005. Spef1, a conserved novel testis protein found in mouse sperm flagella. *Gene.* 353:189–199. https://doi.org/10.1016/j.gene.2005.04.025

Chien, Y.H., R. Keller, C. Kintner, and D.R. Shook. 2015. Mechanical strain determines the axis of planar polarity in ciliated epithelia. *Curr. Biol.* 25:2774–2784. https://doi.org/10.1016/j.cub.2015.09.015

Dougherty, G.W., H.J. Adler, A. Rzadzinska, M. Gimona, Y. Tomita, M.C. Lattig, R.C. Merritt Jr., and B. Kachar. 2005. CLAMP, a novel microtubule-associated protein with EB-type calponin homology. *Cell Motil. Cytoskeleton.* 62:141–156. https://doi.org/10.1002/cm.20093

Goodrich, L.V., and D. Strutt. 2011. Principles of planar polarity in animal development. *Development.* 138:1877–1892. https://doi.org/10.1242/dev.054080

Guirao, B., A. Meunier, S. Mortaud, A. Aguilar, J.M. Corsi, L. Strehl, Y. Hirota, A. Desoeuvre, C. Boutin, Y.G. Han, et al. 2010. Coupling between hydrodynamic forces and planar cell polarity orients mammalian motile cilia. *Nat. Cell Biol.* 12:341–350. https://doi.org/10.1038/ncb2040

Hendershott, M.C., and R.D. Vale. 2014. Regulation of microtubule minus-end dynamics by CAMSAPs and Patronin. *Proc. Natl. Acad. Sci. USA.* 111:5860–5865. https://doi.org/10.1073/pnas.1404133111

Jiang, K., S. Hua, R. Mohan, I. Grigoriev, K.W. Yau, Q. Liu, E.A. Katrukha, A.F. Altelaar, A.J. Heck, C.C. Hoogenraad, and A. Akhmanova. 2014. Microtubule minus-end stabilization by polymerization-driven CAMSAP deposition. *Dev. Cell.* 28:295–309. https://doi.org/10.1016/j.devcel.2014.01.001

Klos Dehring, D.A., E.K. Vladar, M.E. Werner, J.W. Mitchell, P. Hwang, and B.J. Mitchell. 2013. Deuterosome-mediated centriole biogenesis. *Dev. Cell.* 27:103–112. https://doi.org/10.1016/j.devcel.2013.08.021

Mitchell, B., R. Jacobs, J. Li, S. Chien, and C. Kintner. 2007. A positive feedback mechanism governs the polarity and motion of motile cilia. *Nature.* 447:97–101. https://doi.org/10.1038/nature05771

Mitchell, B., J.L. Stubbs, F. Huisman, P. Taborek, C. Yu, and C. Kintner. 2009. The PCP pathway instructs the planar orientation of ciliated cells in the Xenopus larval skin. *Curr. Biol.* 19:924–929. https://doi.org/10.1016/j.cub.2009.04.018

Park, T.J., B.J. Mitchell, P.B. Abitua, C. Kintner, and J.B. Wallingford. 2008. Dishevelled controls apical docking and planar polarization of basal bodies in ciliated epithelial cells. *Nat. Genet.* 40:871–879. https://doi.org/10.1038/ng.104

Shimada, Y., S. Yonemura, H. Ohkura, D. Strutt, and T. Uemura. 2006. Polarized transport of Frizzled along the planar microtubule arrays in Drosophila wing epithelium. *Dev. Cell.* 10:209–222. https://doi.org/10.1016/j.devcel.2005.11.016

Sive, H.L., R.M. Grainger, and R.M. Harland. 1998. The Early Development of Xenopus laevis: A Laboratory Manual. Cold Spring Harbor Laboratories, Plainview, New York.

Strutt, H., and D. Strutt. 2008. Differential stability of flamingo protein complexes underlies the establishment of planar polarity. *Curr. Biol.* 18:1555–1564. https://doi.org/10.1016/j.cub.2008.08.063

Strutt, D., R. Schnabel, F. Fiedler, and S. Prömel. 2016. Adhesion GPCRs Govern Polarity of Epithelia and Cell Migration. *Handb. Exp. Pharmacol.* 234:249–274. https://doi.org/10.1007/978-3-319-41523-9_11

Stubbs, J.L., E.K. Vladar, J.D. Axelrod, and C. Kintner. 2012. Multicilin promotes centriole assembly and ciliogenesis during multiciliate cell differentiation. *Nat. Cell Biol.* 14:140–147. https://doi.org/10.1038/ncb2406

Tissir, F., and A.M. Goffinet. 2013. Atypical cadherins Celsr1-3 and planar cell polarity in vertebrates. *Prog. Mol. Biol. Transl. Sci.* 116:193–214. https://doi.org/10.1016/B978-0-12-394311-8.00009-1

Vichas, A., and J.A. Zallen. 2011. Translating cell polarity into tissue elongation. *Semin. Cell Dev. Biol.* 22:858–864. https://doi.org/10.1016/j.semcdb.2011.09.013

Vladar, E.K., R.D. Bayly, A.M. Sangoram, M.P. Scott, and J.D. Axelrod. 2012. Microtubules enable the planar cell polarity of airway cilia. *Curr. Biol.* 22:2203–2212. https://doi.org/10.1016/j.cub.2012.09.046

Wallingford, J.B. 2005a. Neural tube closure and neural tube defects: studies in animal models reveal known knowns and known unknowns. *Am. J. Med. Genet. C. Semin. Med. Genet.* 135C:59–68. https://doi.org/10.1002/ajmg.c.30054

Wallingford, J.B. 2005b. Vertebrate gastrulation: polarity genes control the matrix. *Curr. Biol.* 15:R414–R416. https://doi.org/10.1016/j.cub.2005.05.029

Wallingford, J.B., S.E. Fraser, and R.M. Harland. 2002. Convergent extension: the molecular control of polarized cell movement during embryonic development. *Dev. Cell.* 2:695–706. https://doi.org/10.1016/S1534-5807(02)00197-1

Werner, M.E., and B.J. Mitchell. 2012. Understanding ciliated epithelia: The power of Xenopus. *Genesis.* 50:176–185.

Werner, M.E., and B.J. Mitchell. 2013. Using Xenopus skin to study cilia development and function. *Methods Enzymol.* 525:191–217. https://doi.org/10.1016/B978-0-12-397944-5.00010-9

Werner, M.E., P. Hwang, F. Huisman, P. Taborek, C.C. Yu, and B.J. Mitchell. 2011. Actin and microtubules drive differential aspects of planar cell polarity in multiciliated cells. *J. Cell Biol.* 195:19–26. https://doi.org/10.1083/jcb.201106110

Werner, M.E., J.W. Mitchell, W. Putzbach, E. Bacon, S.K. Kim, and B.J. Mitchell. 2014. Radial intercalation is regulated by the Par complex and the microtubule-stabilizing protein CLAMP/Spef1. *J. Cell Biol.* 206:367–376. https://doi.org/10.1083/jcb.201312045

Zhang, S., and B.J. Mitchell. 2015. Centriole biogenesis and function in multiciliated cells. *Methods Cell Biol.* 129:103–127. https://doi.org/10.1016/bs.mcb.2015.03.015